Optimal phase-selective entrainment of heterogeneous oscillator ensembles *

Bharat Singhal†, István Z. Kiss‡, and Jr-Shin Li†§

Abstract. We develop a framework to design optimal entrainment signals that entrain an ensemble of heterogeneous nonlinear oscillators, described by phase models, at desired phases. We explicitly take into account heterogeneity in both oscillation frequency and the type of oscillators characterized by different Phase Response Curves. The central idea is to leverage the Fourier series representation of periodic functions to decode a phase-selective entrainment task into a quadratic program. We demonstrate our approach using a variety of phase models, where we entrain the oscillators into distinct phase patterns. Also, we show how the generalizability gained from our formulation enables us to meet a wide range of design objectives and constraints, such as minimum-power, fast entrainment, and charge-balanced controls.

Key words. Oscillators, Entrainment, Phase model, Synchronization

MSC codes. 37N25, 37N35, 92B25, 34C15, 34C29

1. Introduction.

One of the most pronounced attributes of the natural ecosystem is the synchronization of physiological rhythms to daily or seasonal environmental cycles [43]. This process of synchronizing oscillatory units to external periodic stimuli is known as entrainment or frequency locking, which has been at the core of the sleep, temperature, and hormonal cycles displayed by vertebrates [43, 25, 26]. Other instances of entrainment include entertainment of pancreatic cells to the oscillatory blood glucose level [23], neocortical neurons to the hippocampal theta rhythm [28], electrochemical oscillators to periodic input [18], and environmental cycles driving plant growth [20]. Along with the entrainment, the phase at which a system entrains with a periodic input is also of critical importance. For example, irregularities in the circadian phase of entrainment result in delayed or advanced sleep-phase syndromes [7, 44, 41]. For this reason, it is crucial to study entrainment and design periodic signals that can entrain heterogeneous oscillators at desired entrainment phases.

Furthermore, in certain biological systems, specific collective behavior of the underlying nonlinear oscillators is required to attain the appropriate functioning. For instance, synchronization of cellular elements generates rhythms in nervous systems [5], and firing patterns of neurons characterize memory formation [13]. Disruptions in the system's natural structure lead to pathological conditions such as Parkinson's disease [39], epilepsy [19], and schizophrenia [30], in which excessive synchronization of neuronal activities can be detected. A desired dynamical pattern in an oscillator population, such as in-phase synchronization, cluster formation, or complete desynchronization, can be produced using phase-selective entrainment,

*Submitted on February 22, 2023.

Funding: This work is supported in part by the NSF award CMMI-1933976, the NIH grant R01GM131403-01, and the AFOSR award FA9550-21-1-0335.

†Electrical and Systems Engineering, Washington University in St. Louis, St. Louis, Missouri 63130, USA.

‡Department of Chemistry, Saint Louis University, St. Louis, Missouri 63103, USA.

§Division of Biology & and Biomedical Sciences, Washington University in St. Louis, St. Louis, Missouri 63130, USA.

that is, by entraining each oscillator at a specific phase. For example, all the oscillators in an ensemble can be synchronized by entraining them at identical phases.

The computational and theoretical challenges in using the full state-space models for control design stem from (i) accessibility of partial states, such as local field potentials, for measurement, which makes identification of the state-space model difficult [36], and (ii) the high dimensionality which hinders the control design, assuming that the true model can even be obtained. For this reason, phase models, describing the dynamics of phase defined in the vicinity of the oscillator's limit cycle, are frequently used to investigate oscillatory systems owing to their simplicity [43, 25, 16]. These models are characterized by the natural oscillation frequency and the Phase Response Curve (PRC) of the oscillator. PRC quantifies the variations in the oscillator phase when an input is applied and can be measured experimentally [6, 42].

In literature, several methods have been proposed to entrain a single oscillator or an ensemble of oscillators [48, 47, 41, 40]. The optimal control design to entrain an ensemble of oscillators with identical PRCs is considered in [48]. The problems of fast entrainment and entrainment of an oscillator with uncertain dynamics are also studied [47, 15, 41]. All of the above methods focus only on entraining the oscillators; the phase of entrainment is often not considered. The problem of phase-selective entrainment, which pertains to entraining each oscillator at a certain phase, was analyzed with phase models [49]; the proposed method was applicable for an oscillator population with identical PRCs and the designed entrainment controls are not optimal.

These recent advancements, however, did not take the heterogeneities across oscillators into account, which is a distinct feature in complex networks of biological and social systems [38, 27]. For instance, cortical pyramidal neurons in layer 5 and in layers 2 or 3 have different PRC types [31, 34]. The periodically firing mitral cells in the olfactory bulb exhibit a broad range of PRCs [4]. In [35], the experimentally obtained PRCs in the neocortex and thalamus region are found to be different. In biology, the circadian system in Gonyaulax is composed of two different types of oscillators having different phase response curves [21]. Half-center oscillators (HCOs), which are integral to central pattern generator circuits and are modeled by a pair of Morris-Lecar-type neurons connected by strong fast inhibitory synapses, also exhibit different phase response curves [46].

In this paper, to overcome these current limitations and accommodate practical applications, we build upon the entrainment technique proposed in our previous work [49] and propose a general framework to design optimal stimuli that entrain an ensemble of heterogeneous oscillators with non-identical PRCs at desired phases. Specifically, we decode the optimal entrainment control design problem into a quadratic optimization program by exploiting the periodicity of the system dynamics and using Fourier decomposition. This optimization formulation offers increased flexibility in designing entrainment signals. Specifically, we can entrain different types of oscillators while simultaneously ensuring minimum power and charge neutrality of the input, and furthermore accommodate the trade-off between different objectives such as control power and entrainment errors. For special cases, including single and two-oscillator systems, analytic expressions of optimal controls can be derived by applying the proposed theory. The proposed approach to transform the continuous-time optimal entrainment control problem into a discrete optimization problem is scalable to optimally entrain a large oscillator ensemble.

The organization of the paper is as follows. In section 2, we discuss the phase coordinate transformation for a nonlinear oscillator. In section 3, we leverage the phase model description of an oscillator ensemble to develop the phase-selective entrainment conditions. Section 4 uses the entrainment conditions developed in section 3 to transform the entrainment signal design problem into a quadratic optimization program. In section 5, we extend the control design methodology to a network of coupled heterogeneous oscillators. Finally, in section 6, we discuss several details and implications of our work.

2. Phase models.

Our method is based on the phase model description of a population of oscillators with a common external input. Consider a n-dimensional ($n \geq 2$) system described by a smooth ordinary differential equation

$$\dot{x} = f(x, u), \qquad x(0) = x_0, \tag{2.1}$$

where $x \in \mathbb{R}^n$ is the state of the system, $u \in \mathbb{R}$ is the control input, and the system has an unforced attractive limit cycle $\gamma(t) = \gamma(t+T)$ which satisfies $\dot{\gamma} = f(\gamma, 0)$ on a periodic orbit $\Gamma = \{y \in \mathbb{R}^n : y = \gamma(t) \text{ for } 0 \leq t \leq T\} \subset \mathbb{R}^n$. Suppose the deviations in $x(t)$ from the unforced trajectory $\gamma(t)$ caused by the application of weak external input $u(t)$ are small. In that case, we can obtain a reduced one-dimensional system that accurately captures the dynamics of the original multi-dimensional system. The reduced one-dimensional model, known as the phase model, can be inferred experimentally for a system with unknown dynamics [32, 17, 24]. In a case where system dynamics are known, phase models can also be computed analytically using the phase reduction theory [25]. The phase models are widely employed to study synchronization phenomena of circadian rhythms [12], chemical oscillators [17, 16], and neurons [11].

Using phase reduction theory, the phase dynamics of each unit in an ensemble of N non-identical uncoupled limit-cycle oscillators can be described by

$$\dot{\psi}_j(t) = \omega_j + Z_j(\psi_j)u(t), \qquad j = 1, \ldots, N, \tag{2.2}$$

where $\omega_j = 2\pi/T_j$ is the natural frequency of oscillator j with period T_j and $Z_j(\psi_j)$ is the corresponding Phase Response Curve. PRC characterizes the response of the oscillator phase to weak inputs. PRC can be determined experimentally for an oscillatory system with unknown dynamics [6, 42] or numerically when oscillator dynamics are known [25].

3. Phase-selective entrainment.

Entrainment occurs when an oscillator is synced with a periodic external input, and the phase difference between the oscillator and the external stimulus following entrainment is referred to as the phase of entrainment [26]. The goal of phase-selective entrainment is to design an external periodic input that entrains a set of oscillators to form a prescribed phase distribution. The objective of phase-selective entrainment has implications in treating neurological disorders, such as Parkinson's disease, where desynchronization of oscillators is required to mitigate tremors, and in circadian biology, where a well-adjusted phase of entrainment is crucial for an organism's fitness.

Here, we aim to engineer an optimal periodic input, e.g., minimum-power control, of a given frequency Ω such that the oscillators in the ensemble are entrained at desired entrainment phases $\varphi_1^*, \ldots, \varphi_N^* \in [0, 2\pi)$. To begin, we introduce a slow phase variable by $\varphi_j(t) = \psi_j(t) - \Omega t$,

which is the phase difference between oscillator j and the external input u [49]. The time evolution of the slow phase variable is then given by

$$\dot{\varphi}_j = \Delta\omega_j + Z_j(\varphi_j + \Omega t)u(\Omega t), \qquad j = 1, \ldots, N, \tag{3.1}$$

where $\Delta\omega_j = \omega_j - \Omega$ is the frequency difference between oscillator j and the control input and is called the frequency detuning. The phase difference dynamics in (3.1) is a time-varying system, and thus difficult to analyze. However, the time dependency can be removed if the forcing frequency Ω is sufficiently close to the natural frequencies of the oscillators, i.e., $\Delta\omega_j \ll \Omega$ for $j = 1, \ldots, N$. This follows from the averaging theory that the phase drift $\varphi_j(t)$ will have slower dynamics than the input signal if $\Delta\omega_j \ll \Omega$, and the average effect of the input over one cycle can adequately describe the evolution of $\varphi_j(t)$ [14]. As a result, the phase difference $\varphi_j(t)$ follows a time-invariant dynamic equation

$$\dot{\varphi}_j = \Delta\omega_j + \Lambda_{u,j}(\varphi_j), \tag{3.2}$$

where the interaction function with respect to the input u,

$$\Lambda_{u,j}(\varphi_j) = \frac{1}{2\pi}\int_0^{2\pi} Z_j(\theta + \varphi_j)u(\theta)d\theta \tag{3.3}$$

is a 2π-periodic function, which quantifies the average phase shift due to periodic input over time $T = 2\pi/\Omega$. Upon entrainment, the phase difference between the oscillators and the control input will become constant, resulting in $\dot{\varphi}_j = 0$ for $j = 1, \ldots, N$. Thus, in order to entrain the oscillator j at a phase difference φ_j^*, the resulting interaction function $\Lambda_{u,j}$ must satisfy

$$\begin{aligned} \Delta\omega_j + \Lambda_{u,j}(\varphi_j^*) &= 0, \\ \Lambda'_{u,j}(\varphi_j^*) &\leq 0, \qquad j = 1, \ldots, N, \end{aligned} \tag{3.4}$$

where $\Lambda'_{u,j}$ denotes the first-order derivative of $\Lambda_{u,j}$. The condition $\Lambda'_{u,j}(\varphi_j^*) \leq 0$ is added to ensure the stability of entrainment, and $\Lambda'_{u,j}(\varphi_j^*) = 0$ denotes the marginally stable case. It is important to note that oscillator j will entrain at φ_j^* regardless of the initial phase difference between the oscillator j and control input if φ_j^* is the only phase satisfying (3.4), i.e., designed interaction function $\Lambda_{u,j}$ intersects the horizontal line $-\Delta\omega_j$ only once with negative slope (Figure 3.1(a)). In the case of multiple such intersection points, the entrainment phase will depend on the initial phase difference between the oscillator j and control input as shown in Figure 3.1(b), where the entrainment phase will be φ_j^* only if the initial phase difference is in the grey region. If the initial phase difference is in the blue region, then the oscillator will entrain at the phase φ'_j. The dependency of the entrainment phase on the initial phase can be eliminated by introducing additional constraints on the interaction function, which will be discussed in Section 4.6. In the following, we leverage the Fourier series representation of periodic functions to devise an optimal periodic input with desired frequency so that the resulting interaction functions satisfy the entrainment constraints.

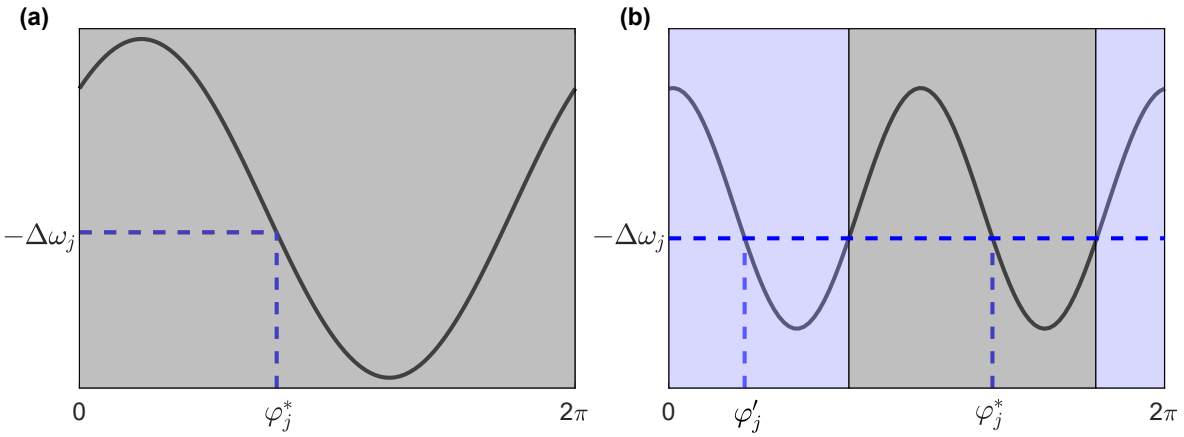

Figure 3.1. *Dependence of the entrainment phase on the initial phase difference. Panel (a) illustrates the case when the interaction function results in a unique entrainment phase φ_j^* for an oscillator with $-\Delta\omega_j$ frequency detuning. For initial phases in the grey region, the entrainment phase will be φ_j^*. Panel (b) depicts the case of multiple entrainment phases depending on the initial phase. For initial phases in grey (resp. blue), the entrainment phase will be φ_j^* (resp. φ_j').*

4. Principle of optimal entrainment control design. In many applications, described in Section 1, it is desirable to entrain oscillators at a specified phase configuration by designing an optimal entrainment signal, such as minimum-power control. We accomplish this by transforming the optimal control design into a convex optimization problem, with the control power as the objective function and the entrainment conditions as constraints, by leveraging the Fourier series representation of periodic functions.

4.1. Fourier representation of the interaction function. For an ensemble of oscillators with given PRCs, each PRC can be approximated using the Fourier series with arbitrary accuracy, owing to the fact that the PRC is a 2π-periodic function. Using Fourier series, we can express the PRC of oscillator j as

$$Z_j(\theta) \approx F_j(\theta) \doteq a_{0,j} + \sum_{n=1}^{r_j} [a_{n,j}\cos(n\theta) + b_{n,j}\sin(n\theta)], \tag{4.1}$$

where the number of Fourier terms, r_j, determines the accuracy of the approximation; namely $\|Z_j - F_j\|_2 = \int_{\theta=0}^{2\pi} (Z_j(\theta) - F_j(\theta))^2 d\theta \leq \varepsilon$. Additionally, the control input $u(\theta)$ is a 2π-periodic function; thus, it can also be expressed using the Fourier series as

$$u(\theta) = c_0 + \sum_{n=1}^{r} [c_n\cos(n\theta) + d_n\sin(n\theta)], \tag{4.2}$$

where the coefficients $c_0, \{c_i, d_i\}_{i=1}^{r}$, and the number of harmonics r are to be determined. Plugging (4.1) and (4.2) into (3.3) yields interaction function of oscillator j,

$$\Lambda_{u,j}(\varphi) = f_{0,j} + \sum_{n=1}^{\min(r,r_j)} [f_{n,j}\cos(n\varphi) + g_{n,j}\sin(n\varphi)], \tag{4.3}$$

where the Fourier coefficients are given by

$$f_{0,j} = a_{0,j}c_0, \qquad f_{n,j} = \frac{a_{n,j}c_n + b_{n,j}d_n}{2}, \qquad g_{n,j} = \frac{b_{n,j}c_n - a_{n,j}d_n}{2}. \tag{4.4}$$

We now define a new variable $r^* = \max(r_1, \ldots, r_N)$, the maximum number of harmonics among the PRCs represented via Fourier series. It can be argued that the minimum-power control will have r^* harmonics, i.e., $r = r^*$. To see this, note that if the control contains more than r^* harmonics, then from (4.3) the interaction function contains only r_j harmonics, and the additional input harmonics will increase the input power. In contrast, a control with less than r^* harmonics results in a smaller number of candidate interaction functions that satisfy entrainment criteria.

4.2. Optimization formulation for control design. Let i be the index of the oscillator with the largest number of Fourier harmonics in its PRC, i.e., $r_i = r^*$. Using (4.4), we can express the Fourier coefficients of the input signal $u(\theta)$ as a function of the Fourier coefficients of the PRC and interaction function of oscillator i, given by

$$\begin{aligned} c_0 &= \frac{f_{0,i}}{a_{0,i}}\chi_{[a_{0,i}\neq 0]}, \qquad c_n = 2\frac{f_{n,i}a_{n,i} + b_{n,i}g_{n,i}}{a_{n,i}^2 + b_{n,i}^2}\chi_{[a_{n,i}^2+b_{n,i}^2\neq 0]}, \\ d_n &= 2\frac{f_{n,i}b_{n,i} - a_{n,i}g_{n,i}}{a_{n,i}^2 + b_{n,i}^2}\chi_{[a_{n,i}^2+b_{n,i}^2\neq 0]}, \end{aligned} \tag{4.5}$$

where $\chi_C = 1$ if the condition C is true; otherwise $\chi_C = 0$. This relation between the input and the interaction function allows us to determine the input power in terms of the Fourier coefficients of the interaction function. By defining $\boldsymbol{x} = [\sqrt{2}c_0, c_1, d_1, \ldots, d_r]$ and $\boldsymbol{y} = [f_{0,i}, f_{1,i}, g_{1,i}, \ldots, g_{r,i}]$, the input power can be expressed as $\mathbb{P}_u = \frac{1}{2\pi}\int_{2\pi} u^2(\theta)d\theta = \frac{1}{2}\boldsymbol{x}^T\boldsymbol{x}$ using Parseval's theorem [22]. From (4.5), we further obtain $\mathbb{P}_u = \frac{1}{2}\boldsymbol{x}^T\boldsymbol{x} = \frac{1}{2}\boldsymbol{y}^T Q\boldsymbol{y}$, where $Q \in \mathbb{R}^{(2r+1)\times(2r+1)}$ is a diagonal matrix with non-negative entries such that the k^{th} diagonal entry,

$$[Q]_{kk} = \begin{cases} \frac{2}{a_{0,i}^2}\chi_{[a_{0,i}\neq 0]}, & k = 1 \\ \frac{4}{a_{m,i}^2+b_{m,i}^2}\chi_{[a_{m,i}^2+b_{m,i}^2\neq 0]}, & k > 1 \end{cases}, \tag{4.6}$$

and $m = \lfloor \frac{k}{2} \rfloor$.

In addition to deriving the relationship between $\mathbb{P}_u$ and $\Lambda_{u,i}$, we establish the relationship between $\Lambda_{u,i}$ and $\Lambda_{u,j}$ for $j = 1, \ldots, N$ and $j \neq i$. This will enable us to transform the control design into an optimization problem with $\boldsymbol{y}$ ($\Lambda_{u,i}$) as a decision variable. Specifically, we observe that for an ensemble controlled by a single control input, the variation in oscillator

interaction functions is attributable to the variability of the PRCs, as the interaction function depends on the PRC and the control input, with the latter being identical for the ensemble. In other words, if we know the interaction function of an oscillator, we can determine the interaction functions of any other oscillators in the ensemble and represent each of them as a function of the known interaction function. This can be done by first estimating the control input from the known interaction function and then using the estimated control input to evaluate the remaining interaction functions. Using (4.5) and (4.4), we get

$$\begin{aligned} f_{0,j} &= \frac{a_{0,j}}{a_{0,i}} f_{0,i}\chi_{[a_{0,i}\neq 0]}, \qquad f_{n,j} \;\; = \alpha_{n,j} f_{n,i} + \beta_{n,j} g_{n,i}, \\ g_{n,j} &= -\beta_{n,j} f_{n,i} + \alpha_{n,j} g_{n,i}, \qquad j = 1, \ldots, N, \end{aligned} \tag{4.7}$$

where

$$\alpha_{n,j} = \frac{a_{n,i}a_{n,j} + b_{n,i}b_{n,j}}{a_{n,i}^2 + b_{n,i}^2}\chi_{[a_{n,i}^2+b_{n,i}^2\neq 0]}, \qquad \beta_{n,j} = \frac{b_{n,i}a_{n,j} - a_{n,i}b_{n,j}}{a_{n,i}^2 + b_{n,i}^2}\chi_{[a_{n,i}^2+b_{n,i}^2\neq 0]}.$$

Consequently, we can express the entrainment conditions, (3.4), in the matrix form as

$$\begin{aligned} A\boldsymbol{y} &= \boldsymbol{b}, \\ G\boldsymbol{y} &\leq \boldsymbol{0}, \end{aligned} \tag{4.8}$$

where the vector $\boldsymbol{b} = [-\Delta\omega_1, \ldots, -\Delta\omega_N]$ represents the frequency detuning for each oscillator in the ensemble, and the matrices $A, G \in \mathbb{R}^{N\times(2r+1)}$ satisfy $(A)_j\boldsymbol{y} = \Lambda_{u,j}(\varphi_j^*)$ and $(G)_j\boldsymbol{y} = \Lambda'_{u,j}(\varphi_j^*)$, with $(A)_j$ and $(G)_j$ denoting the j^{th} row of the matrix A and G; namely,

$$(A)_j = \begin{bmatrix} \frac{a_{0,j}}{a_{0,i}} \\ \alpha_{1,j}\cos(\varphi_j^*) - \beta_{1,j}\sin(\varphi_j^*) \\ \alpha_{1,j}\sin(\varphi_j^*) + \beta_{1,j}\cos(\varphi_j^*) \\ \vdots \\ \alpha_{r,j}\cos(r\varphi_j^*) - \beta_{r,j}\sin(r\varphi_j^*) \\ \alpha_{r,j}\sin(r\varphi_j^*) + \beta_{r,j}\cos(r\varphi_j^*) \end{bmatrix}^T, \quad (G)_j = \begin{bmatrix} 0 \\ -\alpha_{1,j}\sin(\varphi_j^*) - \beta_{1,j}\cos(\varphi_j^*) \\ \alpha_{1,j}\cos(\varphi_j^*) - \beta_{1,j}\sin(\varphi_k^*) \\ \vdots \\ -r\alpha_{r,j}\sin(r\varphi_j^*) - r\beta_{r,j}\cos(r\varphi_k^*) \\ r\alpha_{r,j}\cos(r\varphi_j^*) - r\beta_{r,j}\sin(r\varphi_j^*) \end{bmatrix}^T.$$

Furthermore, we introduce $\boldsymbol{h} = [h_1, \ldots, h_N]$ $(h_j \leq 0)$ to confine the slope of the interaction functions at the fixed points φ_j^*, $j = 1, \ldots, N$, by imposing the condition $G\boldsymbol{y} \leq \boldsymbol{h}$. This constraint will ensure a minimum rate of convergence, $|h_j|$, of the phase in the neighborhood of φ_j^*. As a result, the interaction function corresponding to the optimal power control, hereafter referred to as the optimal interaction function, can be obtained by solving the convex optimization problem,

$$\begin{aligned} \min_{\boldsymbol{y}} \quad & \frac{1}{2}\boldsymbol{y}^T Q\boldsymbol{y}, \\ \text{s.t.} \quad & A\boldsymbol{y} = \boldsymbol{b}, \\ & G\boldsymbol{y} \leq \boldsymbol{h}. \end{aligned} \tag{4.9}$$

In general, a closed-form solution cannot be obtained for this quadratic convex optimization problem with inequality constraints; numerical methods, such as interior-point or active-set methods, can be employed to effectively determine a global minimizer [3]. The corresponding minimum-power control can then be obtained by utilizing (4.5).

Remark 4.1. Our optimization framework provides the freedom to regulate the local speed of entrainment while designing the optimal interaction function by appropriately modifying $\boldsymbol{h}$. By increasing the absolute values of h_j, we can achieve faster entrainment due to the increased slope of the interaction function at the fixed point φ_j^* at the cost of increased input power.

Remark 4.2. For some special cases, explicit optimal control expressions can be obtained by (4.9) providing further insights into the underlying entrainment process by elucidating the dependence of the control input on PRC and frequency detuning. For example, minimum-power control to entrain a single oscillator at phase φ^* can be derived as $u(\theta) = -\frac{\Delta\omega}{\langle Z^2\rangle} Z(\theta + \varphi^*) + \frac{h}{\langle Z'^2\rangle} Z'(\theta + \varphi^*)$, where $|h|$ denotes the minimum local speed of entrainment ($G\boldsymbol{y} \leq h$), Z' is the first-order derivative of PRC, and $\langle\cdot\rangle$ is an average operator on 2π-periodic functions (Appendix A). The obtained minimum-power control coincides with the one derived in [47] using calculus of variations. It is worth noting that the closed-form optimal interaction function to marginally entrain all the oscillators in the ensemble, i.e., satisfying $G\boldsymbol{y} = \boldsymbol{0}$ in (4.9), is the minimum-norm solution given by

$$\boldsymbol{y} = Q^{-1}\begin{bmatrix} G^T & A^T \end{bmatrix}\left(\begin{bmatrix} G \\ A \end{bmatrix} Q^{-1}\begin{bmatrix} G^T & A^T \end{bmatrix}\right)^{-1}\begin{bmatrix} \boldsymbol{0} \\ \boldsymbol{b} \end{bmatrix}.$$

4.3. Anti-phase entrainment of two oscillators. In the case of two oscillators, the regular patterns of coordination are well represented by the relative phase between their periodic motions [2]. For example, anti-phase entrainment of two weakly coupled oscillators plays a crucial role in circadian biology where desynchronization of two oscillators in anatomically defined ventrolateral and dorsomedial SCN subdivisions is used to understand SCN tissue organization and signaling mechanisms in animals [9]. From (4.9), the optimal control to entrain two oscillators in an anti-phase configuration is given by (Appendix B)

$$u(\theta) = aZ(\theta + \varphi_1^*) + bZ(\theta + \varphi_2^*), \tag{4.10}$$

where the coefficients a and b are functions of the Fourier coefficients of the PRC and frequency detuning, and φ_1^* and φ_2^* are the entrainment phase of each oscillator such that $\varphi_2^* - \varphi_1^* = \pi$. Note that the optimal power control is simply a linear combination of the shifted PRCs. Figure 4.1 displays the minimum input power required to entrain two oscillators in an anti-phase configuration. Remarkably, the variation of minimum-power with frequency detuning resembles an inverted 3-d cone, which can be thought of as a 3-d version of Arnold Tongue [25].

4.4. Numerical examples. Here, we present two numerical examples showing the optimality and capability of our technique to entrain oscillators with different PRCs. We first demonstrate our proposed theory by entraining an ensemble of four Hodgkin-Huxley phase oscillators [47] with identical PRCs using a periodic input of 10 rad/s frequency such that $\pi/2$ phase difference is assigned between two successive, in terms of frequency, oscillators and the

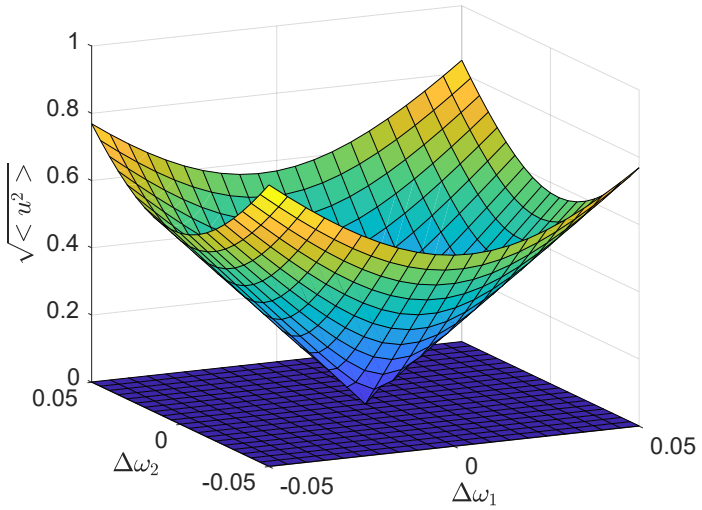

Figure 4.1. *Minimum power of the optimal control for anti-phase entrainment of two oscillators. The conic surface represents the theoretically estimated power of input in* (4.10)*, for anti-phase entrainment of two oscillators (*$\boldsymbol{h} = \mathbf{0}$*). The blue surface denotes the difference between the power of theoretically predicted input and the input obtained by numerically solving the optimization problem* (4.9)*. Both oscillators have Hodgkin-Huxley PRCs and the input frequency is* $10\,rad/s$*.*

slowest oscillator is entrained at phase $\pi/4$ with the input. The frequencies of the oscillators are uniformly distributed between $[9.99, 10.01]$ rad/s. The PRC is fitted using a Fourier series with five harmonics, and the true and fitted PRCs are illustrated by the dashed blue and solid red lines, respectively, in Figure 4.2(a). After obtaining the Fourier coefficients of the PRC, we construct the matrices A, G, Q and the vector $\boldsymbol{b}$, as described in Section 4, based on the PRC Fourier coefficients, frequency detuning, and the desired entrainment phases. Each entry, h_i, of the vector $\boldsymbol{h}$ is set as -0.01. Following this, the optimal interaction function is obtained by solving the quadratic program in (4.9), using the *quadprog* function in MATLAB. The resulting entrainment phases produced by applying the minimum-power control obtained using the optimal interaction function are depicted in Figure 4.2(d) (colored circles) with the desired phases denoted by the cross sign. The corresponding control input and the interaction function are displayed in Figures 4.2(b) and 4.2(d) by black lines.

The described methodology can achieve significant input power reduction compared to the baseline technique, proposed in [49], which involves first designing a candidate interaction function satisfying the entrainment conditions using a sum of scaled and shifted sigmoid functions and then representing this function using Fourier series. To illustrate this, we repeat the task of designing the control input to entrain the oscillators by using the baseline algorithm. Figure 4.2(c) depicts the designed (dashed blue) and fitted (red line) interaction functions. The control input is shown in Figure 4.2(b) using red color. The assigned phases of each oscillator are shown in Figure 4.2(c) with colored circles. Our method achieves a considerable, about nine-fold input power reduction compared to the baseline method with input power reduces to 0.09 from 0.81.

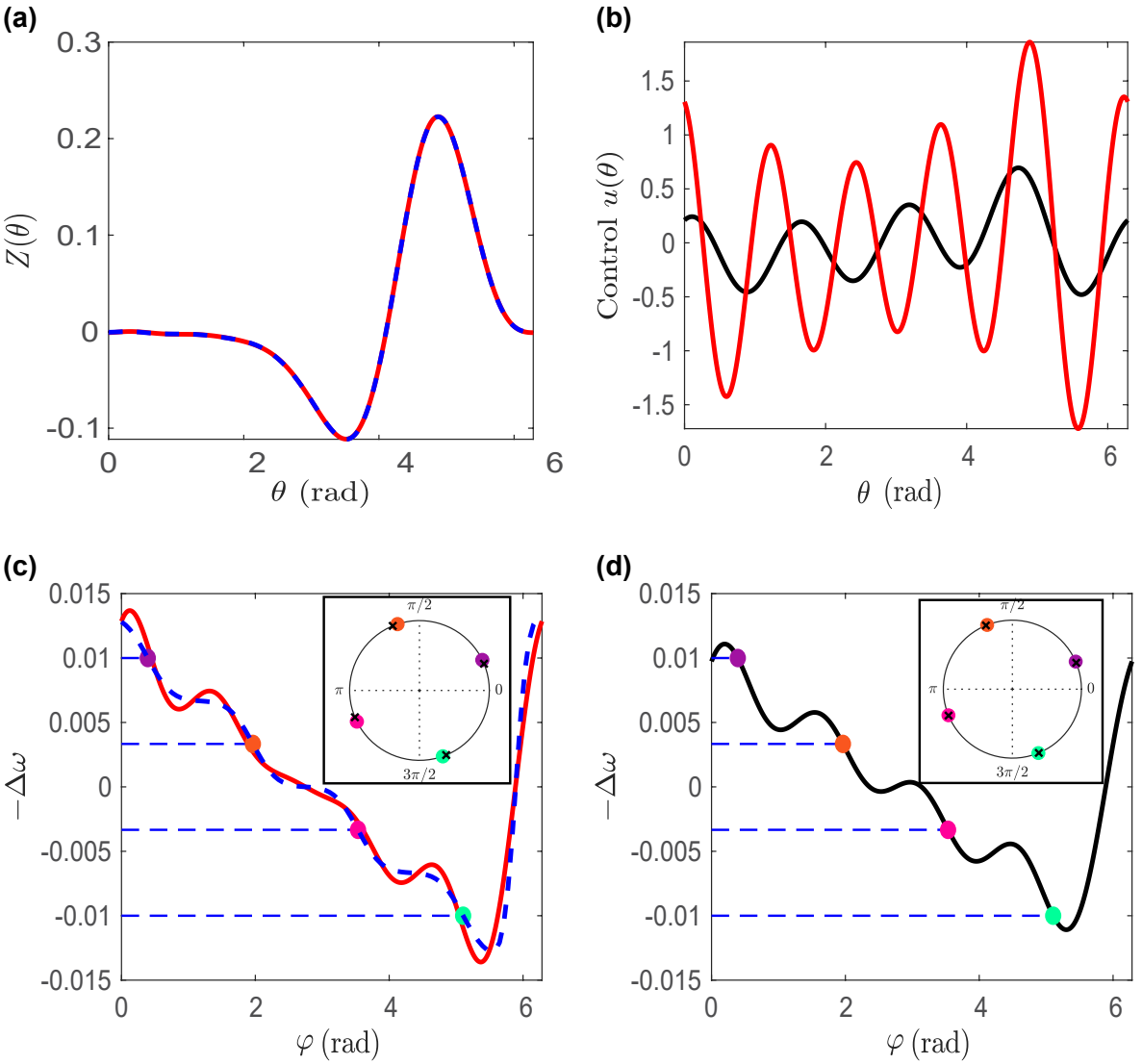

Figure 4.2. *A comparison of the input power between the proposed technique and the baseline technique. (a) True (red line) and fitted PRC (dashed blue) of the four oscillators. For the purpose of the input power comparison, we assume identical PRCs for the oscillators. Panel (b) displays the obtained control input using the baseline technique (red line) and the presented algorithm (black line). Panels (c) and (d) illustrate the designed interaction function and the entrained phases (inset) using the baseline technique and the presented algorithm, respectively. The black crosses and the colored circles denote the desired phases and phases upon entrainment. Designing the control input optimally reduces the input power to* 0.09 *from* 0.81.

The ability of our algorithm to entrain oscillators with different PRCs is illustrated in Figure 4.3, where we entrain two oscillators with Type-1 and Type-2 PRCs at desired phases. Neurons with Type-1 PRC move from rest to tonic spiking via a saddle-node bifurcation, whereas Type-2 PRC neurons transition via a Hopf bifurcation [31, 10]. The phase of a Type-

1 oscillator can only be advanced, while the phase of a Type-2 oscillator can be advanced or delayed depending on the input timing [31]. Figure 4.3(b) depicts a case where we design a periodic input of frequency 10 rad/s to entrain two oscillators with natural frequencies 9.99 and 10.01 rad/s in an in-phase synchronization pattern. To obtain in-phase synchronization between the oscillators, we select identical entrainment phases for each oscillator by choosing $(\varphi_1^*, \varphi_2^*) = (\pi, \pi)$. The slower oscillator has Type-1 PRC, while Type-2 PRC belongs to the faster oscillator. The designed interaction function and the optimal control input are shown in the left and right panels of Figure 4.3(b), where the inset figure displays the entrained oscillator phase on a unit circle. For the same system, we also design a periodic input for anti-phase synchronization of oscillators by entraining the oscillators at $(\varphi_1^*, \varphi_2^*) = (0, \pi)$. The anti-phase synchronization results are displayed in Figure 4.3(c). Note that the obtained phase configurations are independent of the initial conditions of the oscillators since the horizontal lines $-\Delta\omega_j$, $j = 1, 2$, intersect the corresponding interaction functions only once with a negative slope, resulting in a globally attractive fixed point for each oscillator.

Remark 4.3. Note that the entrainment control discussed above is optimal for the given input frequency Ω. In practice, for example, for applications involving synchronization or desynchronization of a network of oscillators, stable phase relations among oscillators are of importance while the entrainment frequency is not a concern. In our framework, the dependence of the optimal control on the input frequency can be readily eliminated by treating Ω as a decision variable in (4.9), formulated as

$$\begin{aligned} \min_{\boldsymbol{y},\Omega} \quad & \frac{1}{2}\boldsymbol{y}^T Q \boldsymbol{y}, \\ \text{s.t.} \quad & \begin{bmatrix} A & -\mathbf{1} \end{bmatrix} \begin{bmatrix} \boldsymbol{y} \\ \Omega \end{bmatrix} = \boldsymbol{b_1}, \\ & \begin{bmatrix} G & \mathbf{0} \end{bmatrix} \begin{bmatrix} \boldsymbol{y} \\ \Omega \end{bmatrix} \leq \boldsymbol{h}, \end{aligned} \tag{4.11}$$

where $-\mathbf{1}, \mathbf{0} \in \mathbb{R}^{2r+1}$ are vectors of -1 and 0, respectively, and $\boldsymbol{b_1} = [-\omega_1, \ldots, -\omega_N]$.

Up to this point, we have provided a convex optimization framework for designing optimal control that entrains an ensemble of oscillators with different PRCs to the desired phase configuration. It is important to note that the feasible region of the quadratic program in (4.9) depends on the nonlinearity of PRCs and the number of oscillators. For instance, as the number of Fourier terms required to approximate the PRCs grows, so does the feasible region and the possibility of the existence of an optimal solution. In contrast, the feasible region is adversely affected by the number of oscillators in the ensemble. To overcome the circumstances when the feasible region is an empty set or too small to find a solution, in the next section, we propose a relaxation in the quadratic program to soften the entrainment conditions by allowing tolerable phase assignment errors using proper regularization in the optimization.

4.5. Regularized phase-selective entrainment of an oscillator ensemble. As the number of oscillators to be entrained increases or the nonlinearity of the PRCs decreases, the feasible set of the optimization problem (4.9) gets smaller, potentially resulting in the case where interaction functions satisfying (3.4) do not exist. This situation can be alleviated by relaxing

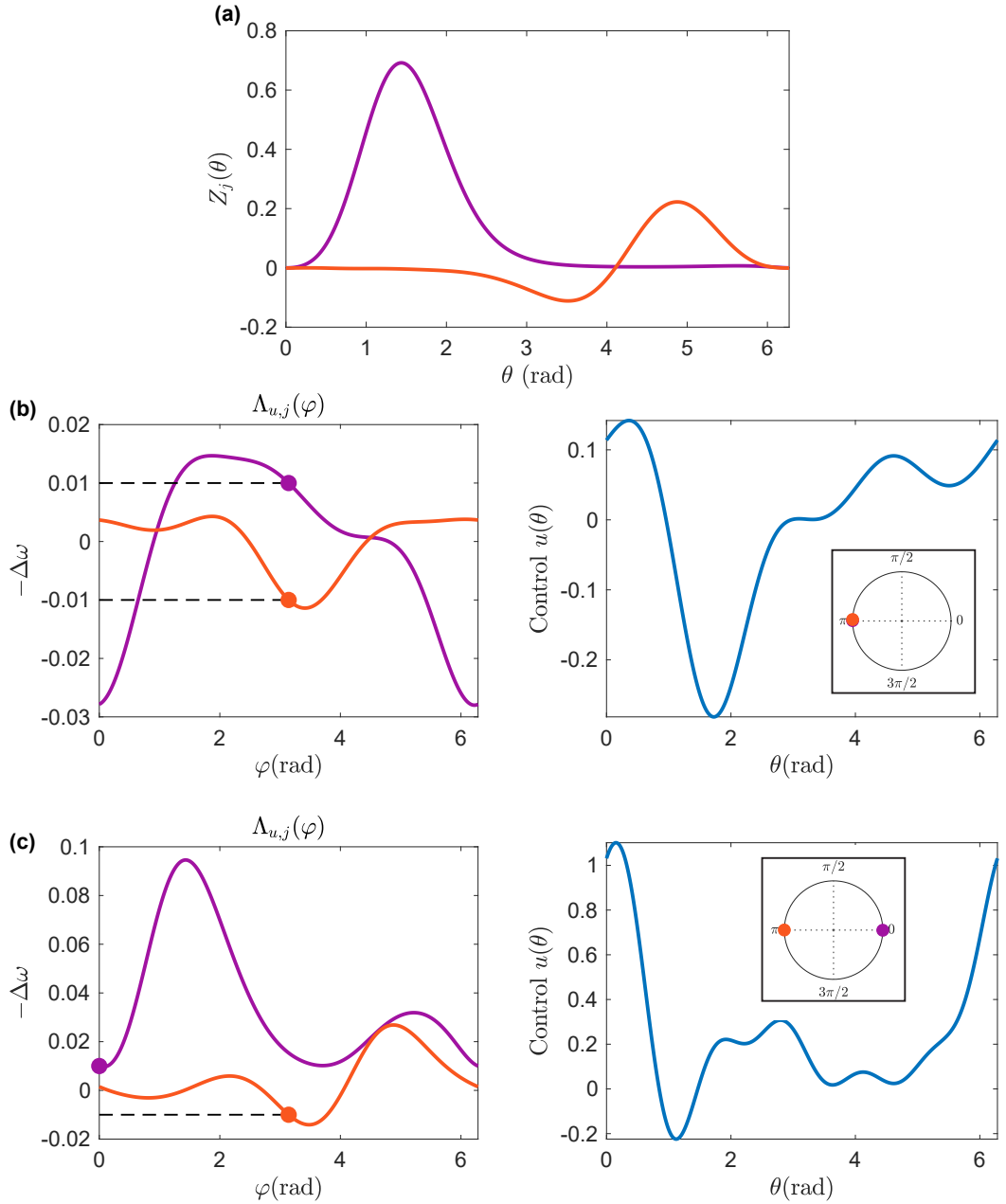

Figure 4.3. *Regulating the phase difference between two oscillators with Type-1 and Type-2 PRCs using convex optimization framework. (a) PRCs of the two oscillators. The left panels in (b) and (c) show the designed interaction functions to achieve in-phase entrainment,* $(\varphi_1^*, \varphi_2^*) = (\pi, \pi)$*, and anti-phase entrainment,* $(\varphi_1^*, \varphi_2^*) = (0, \pi)$*, respectively. The right panels of (b) and (c) illustrate the control inputs, and the entrained oscillator phases on a unit circle (inset) for in-phase and anti-phase entrainment, respectively. We choose* $(\omega_1, \omega_2) = (9.99, 10.01)$ *rad/s shown in (purple,orange) with* $\Omega = 10$ *rad/s. Each entry of vector* $\boldsymbol{h}$ *is set as* -0.01 *for both phase patterns.*

the constraints in (4.9), thereby expanding the feasible region. For example, we can enlarge the feasible region by allowing the interaction functions to pass through the neighborhood of the desired phase differences, $\varphi_1^*, \ldots, \varphi_N^*$, with a negative slope. To this end, we introduce slack variables, $\delta_1, \ldots, \delta_N$, such that

$$\begin{aligned} \Delta\omega_j + \Lambda_{u,j}(\varphi_j^* - \delta_j) &= 0, \\ \Lambda'_{u,j}(\varphi_j^* - \delta_j) &\leq 0, \qquad j = 1, \ldots, N. \end{aligned}$$

The slack variable δ_j corresponds to the phase entrainment error of oscillator j. To avoid large entrainment errors, we modify the objective function to penalize the slack variables. Correspondingly, the optimal interaction function can be obtained by

$$\begin{aligned} \min_{\boldsymbol{y},\boldsymbol{\delta}} \quad & \frac{1}{2}\left(\boldsymbol{y}^T Q \boldsymbol{y} + \lambda \boldsymbol{\delta}^T \boldsymbol{\delta}\right) \\ \text{s.t.} \quad & A(\boldsymbol{\delta})\boldsymbol{y} = \boldsymbol{b}, \\ & G(\boldsymbol{\delta})\boldsymbol{y} \leq \boldsymbol{h}, \end{aligned} \tag{4.12}$$

where the vector $\boldsymbol{\delta} = (\delta_1, \ldots, \delta_N)^T$ contains entrainment phase errors, λ is a regularization parameter, and $\boldsymbol{y}$ comprises the Fourier coefficients of the interaction function. The regularization parameter λ can be used to regulate the phase-assignment errors at the expense of increased input power. Increased value of λ, for example, results in smaller phase-assignment errors but increased input power. In Figure 4.4, we illustrate the input power and phase assignment errors for synchronizing an ensemble of 10 oscillators at $\pi/4$ entrainment phase for 3 distinct values of $\lambda \in \{1, 10, 100\}$.

The matrices $A(\delta)$ and $G(\delta)$ satisfy $(A(\delta))_j \boldsymbol{y} = \Lambda_{u,j}(\varphi_j^* - \delta_j)$ and $(G(\delta))_j \boldsymbol{y} = \Lambda'_{u,j}(\varphi_j^* - \delta_j)$, with $(A(\delta))_j$ and $(G(\delta))_j$ denoting the j^{th} row of the $A(\delta)$ and $G(\delta)$. It is important to note that the regularized optimization problem in (4.12) is not convex because the constraints are non-convex functions. As a result, the optimal solution of (4.12) depends on the initial values of the vectors $\boldsymbol{y}$ and $\boldsymbol{\delta}$.

When PRCs are not sufficiently nonlinear, i.e., containing a small number of harmonics, the technique in [49] may result in large phase entrainment errors. The introduced non-convex optimization formulation will lead to reduced errors by constructing optimal interaction functions that minimize both the input power and entrainment errors.

Remark 4.4. In certain therapeutic applications, such as deep-brain stimulation, it is crucial that external inputs, e.g., currents, applied to stimulate the neurons, are charge-balanced (CB) [42]. Non-charge-balanced stimuli will cause an accumulation of charge over time, which will potentially damage the neural tissues or the surrounding electrodes. The CB constraint can be expressed as $\int_0^T u(t)dt = 0$, where T is the duration of the stimulation [8]. This simply implies $c_0 = 0$ (4.2) and can be directly incorporated in our optimization formulation in (4.12) or (4.9) by constraining the first element of the decision vector, i.e., $\boldsymbol{y}^{(1)} = 0$.

Figure 4.5 demonstrates one such simulation where we entrain an ensemble of 10 oscillators with uniformly distributed frequencies, with the oscillator 1 being the slowest and 10 being the fastest, into two different phase configurations. Oscillators 1-5 have Type-1 PRCs (purple lines,

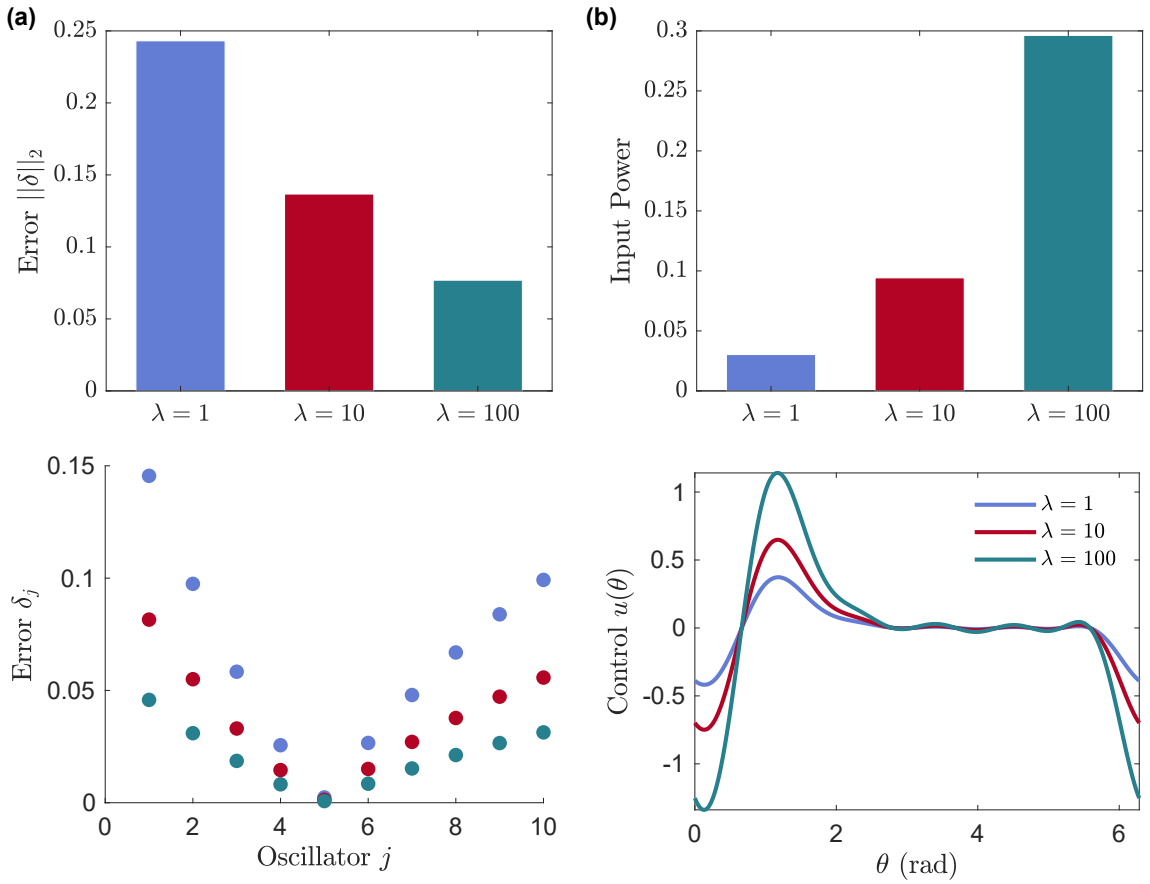

Figure 4.4. *Trade-off between the phase assignment error and input power. The top and bottom figures in panel (a) display the phase entrainment errors for different values of the regularization parameter λ when we design a periodic input of 10 rad/s to synchronize 10 oscillators at $\pi/4$ phase with the input. The top figure of panel (b) shows the corresponding control input power, while the bottom figure displays the obtained control inputs. Each oscillator have Type-1 PRC with different amplitudes, i.e., $Z_i(\psi) = (1 + 0.1(i-1))(1 - \cos(\psi))e^{3(\cos(\psi-\pi/3)-1)}$, and the frequencies of the oscillators are uniformly distributed in $[9.99, 10.01]$ rad/s.*

slower oscillators have smaller amplitude PRCs); oscillators 6-10 have Type-2 PRCs (orange lines). Figure 4.5(b) displays the designed interaction functions to synchronize the oscillator at phase $\pi/4$. The corresponding control input and phases after entrainment are shown in the bottom panel. In Figure 4.5(c), we entrain the ensemble to form two anti-phase clusters at $\pi/4$ and $5\pi/4$. Each entry of vector $\boldsymbol{h}$ and the regularization parameter λ are set as -0.01 and 10, respectively. The phase assignment errors, δ_j, are on the order of 10^{-2}.

4.6. Global phase assignment. In our framework, oscillator j will entrain at phase φ_j^* only if the initial phase offset between the oscillator and the input lies in the region of attraction of the φ_j^*, stable fixed point of (3.2) (Figure 3.1). This implies that the entrainment phase will be independent of the initial phase offset if there is a single stable fixed point, which will

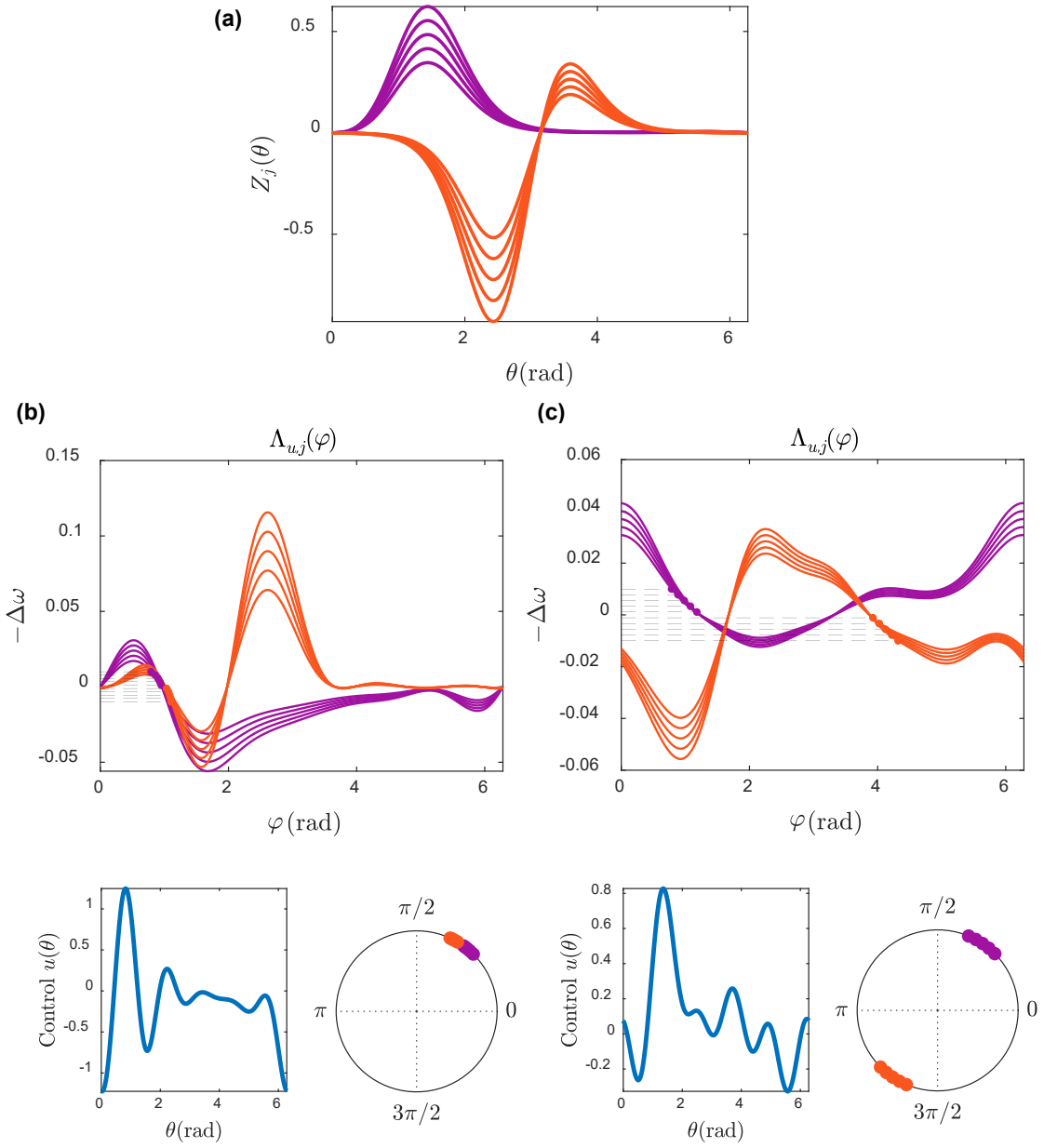

Figure 4.5. *In-phase synchronization and cluster-formation in an oscillator ensemble with heterogeneous PRCs using non-convex optimization framework. (a) PRCs of the oscillators in the network. The top panels of (b) and (c) display the designed optimal interaction functions to synchronize the oscillators at phase* $\pi/4$ *and to construct two clusters at* $\pi/4$ *and* $5\pi/4$ *with 5 oscillators in each cluster. The bottom panels of (b) and (c) illustrate the respective control input (left) and the achieved phase pattern on a unit circle (right). All the oscillators have identical initial phases at 0 and the frequencies are uniformly distributed in* $[9.99, 10.01]$ *rad/s with the oscillator* 1 *being the slowest and* 10 *being the fastest; the periodic input is of frequency* 10 *rad/s.*

occur if $\Lambda_{u,j}(\varphi)$ intersects the horizontal line $-\Delta\omega_j$ exactly twice in the interval $\varphi = [0, 2\pi)$ (the intersection point with the positive slope results in an unstable fixed point).

One naive approach to ensure that each $\Lambda_{u,j}(\varphi)$ intersects the horizontal line $-\Delta\omega_j$ twice would be to derive analytic constraints on the Fourier coefficients of $\Lambda_{u,j}(\varphi)$ and incorporate them in the optimization problem. However, determining the analytic form of the constraints is a challenge in its own right. To bypass this difficulty, we propose a sampling-based method to ensure that the resulting phase patterns are unique, i.e., independent of the initial state of the oscillators. The proposed sampling-based method yields interpretable conditions while avoiding the difficulty of deriving analytic constraints.

The central idea is to sample the function $p_j(\varphi) = \Lambda_{u,j}(\varphi) + \Delta\omega_j$ at M uniformly distributed points in the domain $\varphi = [0, 2\pi)$ and constrain the number of times $p_j(\varphi)$ changes the sign to be equal to 2. This constraint will ensure precisely two intersection points between $\Lambda_{u,j}(\varphi)$ and the horizontal line $-\Delta\omega_j$. Let $\varphi_{1,s}, \varphi_{2,s}, \ldots, \varphi_{M,s}$ be the sampling points, then the unique phase pattern condition can be written in the closed-form as

$$\underbrace{\sum_{k=1}^{M-1} H(-p_j(\varphi_{k,s}).p_j(\varphi_{k+1,s}))}_{\text{Number of sign changes of } p_j(\varphi)} = 2 \qquad j = 1, \ldots, N, \tag{4.13}$$

where H is a logistic function, $H(x) = \frac{1}{1+e^{-\alpha x}}$, with a high enough α to approximate a Heaviside step function [1]. $H(-p_j(\varphi_{k,s}).p_j(\varphi_{k+1,s}))$ will be 1 if the function $p_j(\varphi)$ changes sign between $\varphi_{k,s}$ and $\varphi_{k+1,s}$, and will be 0 otherwise. By incorporating (4.13) as additional constraints in the optimization problem (4.12), we can obtain optimal interaction functions that give us the desired phase pattern regardless of the initial phases.

Figure 4.6 illustrates the effect of including uniqueness constraints (4.13) to entrain the oscillator population at two anti-phase clusters using a periodic input of frequency 0.975 rad/s. We consider two groups of oscillators, having 49 and 50 oscillators with mean frequencies of 0.95 and 1 rad/s, respectively, and the ensemble with smaller frequency has a smaller amplitude PRC (purple line, Figure 4.6(a)). In the absence of uniqueness conditions (Figure 4.6(c)), the interaction functions of the second oscillator population (orange color) result in two stable fixed points, producing two distinct clusters. However, when we include the constraints (4.13), the obtained interaction functions intersect the corresponding horizontal line $-\Delta\omega_j$ only once with a negative slope (Figure 4.6(d)), giving us the desired phases from arbitrary initial conditions. Figure 4.6(b) illustrates the corresponding control input when uniqueness constraints are included (red color) or not included (black color). Inner circles in the left panels of Figures 4.6(c) and (d) denote the initial phase of each oscillator with input.

Remark 4.5. In neuroscience, the typical inputs are pulsatile, for example, deep brain stimulation (DBS) in Parkinsonian patients. To make use of the designed optimal entrainment waveforms, we present a simple technique to implement them as a pulse train. The core idea of our approach is to apply a high-frequency pulse train, such as 200 Hz [45, 37], of narrow pulse width (1 ms), with the pulse amplitude being determined by the reference signal, i.e., control generated by our algorithm, at the instant when pulse is applied (see Appendix C for more details). The designed pulses are then applied to the two numerical examples presented in Section 4.4 and the resulting entrainment phases are shown in Figure C.2.

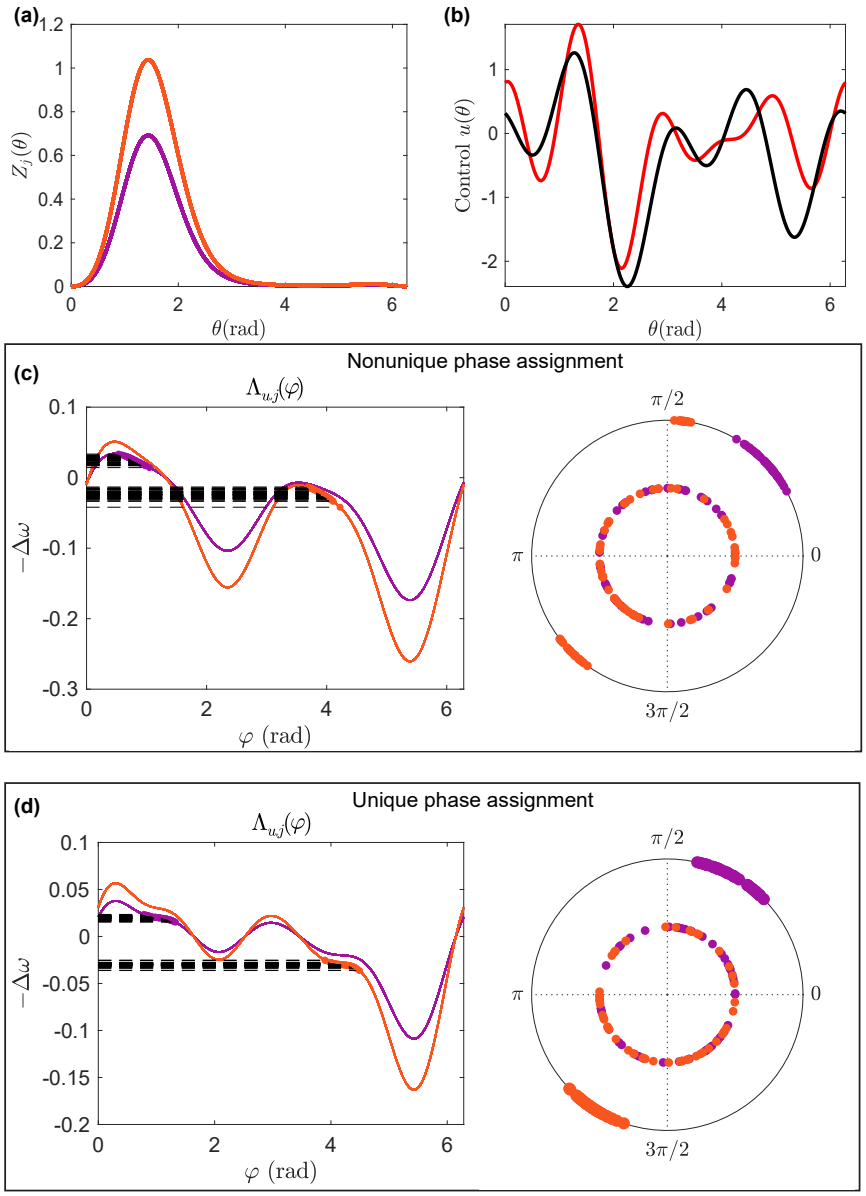

Figure 4.6. *Cluster formation in an ensemble of* 99 *oscillators with Type-1 PRCs. (a) PRCs of the oscillators in the ensemble with each oscillator having the PRC with identical color. (b) Devised periodic control inputs to form clusters. The Red (black) line depicts the input when unique entrainment phase conditions* (4.13) *are added (resp., not added). Left panels of (c) and (d) display the designed interaction functions. The right panels of the (c) and (d) show the achieved phase pattern upon entrainment (outer circle) with the inner circle denoting the initial phase of each oscillator.* 49 *oscillators with mean frequency* $0.95\,rad/s$ *are in cluster-1 (purple). Cluster-2 (orange) contains* 50 *oscillators with mean frequency* $1\,rad/s$ *; forcing frequency* $\Omega = 0.975\,rad/s$.

5. Phase-selective entrainment of coupled oscillators. Thus far, our analysis is focused on the cases of uncoupled oscillators. The extension to the entrainment of coupled oscillators is natural and compelling. This can be directly achieved following the developed framework presented in Section 4. Here, we consider a network of N symmetrically coupled oscillators with the phase dynamics of oscillator j, $j = 1, \ldots, N$, expressed as [29]

$$\dot{\psi}_j(t) = \omega_j + \sum_{\substack{k=1 \\ k\neq j}}^{N} \alpha_{jk}(\psi_j(t) - \psi_k(t)) + Z_j(\psi_j)u(\Omega t), \tag{5.1}$$

where the coupling input to oscillator j from oscillator k is characterized by the coupling function α_{jk} $(= \alpha_{kj})$. If there is no interaction or connection between oscillators j and k, then the coupling functions α_{jk} and α_{kj} are trivially zero. Following the discussion in Section 3, the dynamics of the averaged phase difference between the oscillator j and periodic input can be written as

$$\dot{\varphi}_j = \Delta\omega_j + \sum_{\substack{k=1 \\ k\neq j}}^{N} \alpha_{jk}(\varphi_j(t) - \varphi_k(t)) + \Lambda_{u,j}(\varphi_j). \tag{5.2}$$

Consequently, the interaction functions that entrain the coupled oscillator network at phases $\varphi_1^*, \ldots, \varphi_N^*$ must satisfy

$$\begin{aligned} \Delta\omega_j + \sum_{\substack{k=1 \\ k\neq j}}^{N} \alpha_{jk}(\varphi_j^* - \varphi_k^*) + \Lambda_{u,j}(\varphi_j^*) = 0, \\ \Lambda'_{u,j}(\varphi_j^*) + \kappa \leq 0, \qquad j = 1, \ldots, N, \end{aligned} \tag{5.3}$$

where κ is the largest eigenvalue of the matrix with $(i,j)^{th}$ element as $\sum_{1=k\neq i}^{N} \frac{\partial}{\partial\varphi_j}\alpha_{ik}(\varphi_i^* - \varphi_k^*)$ to ensure the stability of the entrainment phases. Using (5.3), the optimal control can be determined by repeating the procedure outlined in Section 4, with the vectors $\boldsymbol{b}$ and $\boldsymbol{h}$ being modified to include the coupling effects. Specifically, we have $\boldsymbol{b} = [-\Delta\omega_1 - \sum_{1=k\neq 1}^{N} \alpha_{1k}(\varphi_1^* - \varphi_k^*), \ldots, -\Delta\omega_N - \sum_{1=k\neq N}^{N} \alpha_{Nk}(\varphi_N^* - \varphi_k^*)]$ and $\boldsymbol{h} = [h_1 - \kappa, \ldots, h_N - \kappa]$, where the constants $h_j \leq 0$, $j = 1, \ldots, N$, can be used to regulate the local speed of entrainment.

Unique entertainment phases are obtained from arbitrary initial phases if the system of equations (5.3) has only one solution $\varphi_1^*, \ldots, \varphi_N^*$ for the designed interaction functions. When oscillators are uncoupled, it is relatively simple to determine a unique solution to the entrainment conditions, as each oscillator has its own entrainment condition independent of the phase of the other oscillators (Figure 3.1). For the coupled ensemble, the condition to ensure a unique entrainment phase for an oscillator depends on the phases of other oscillators and the coupling functions, rendering the analysis computationally intractable. Nonetheless, our control input will entrain the coupled ensemble, and the entrainment phases will be desired if the initial phases lie in the region of attraction of the desired entrainment phases.

As a numerical example, we entrain a network of 10 coupled oscillators connected in the manner illustrated in Figure 5.1(a). Frequencies of the oscillators are uniformly distributed in

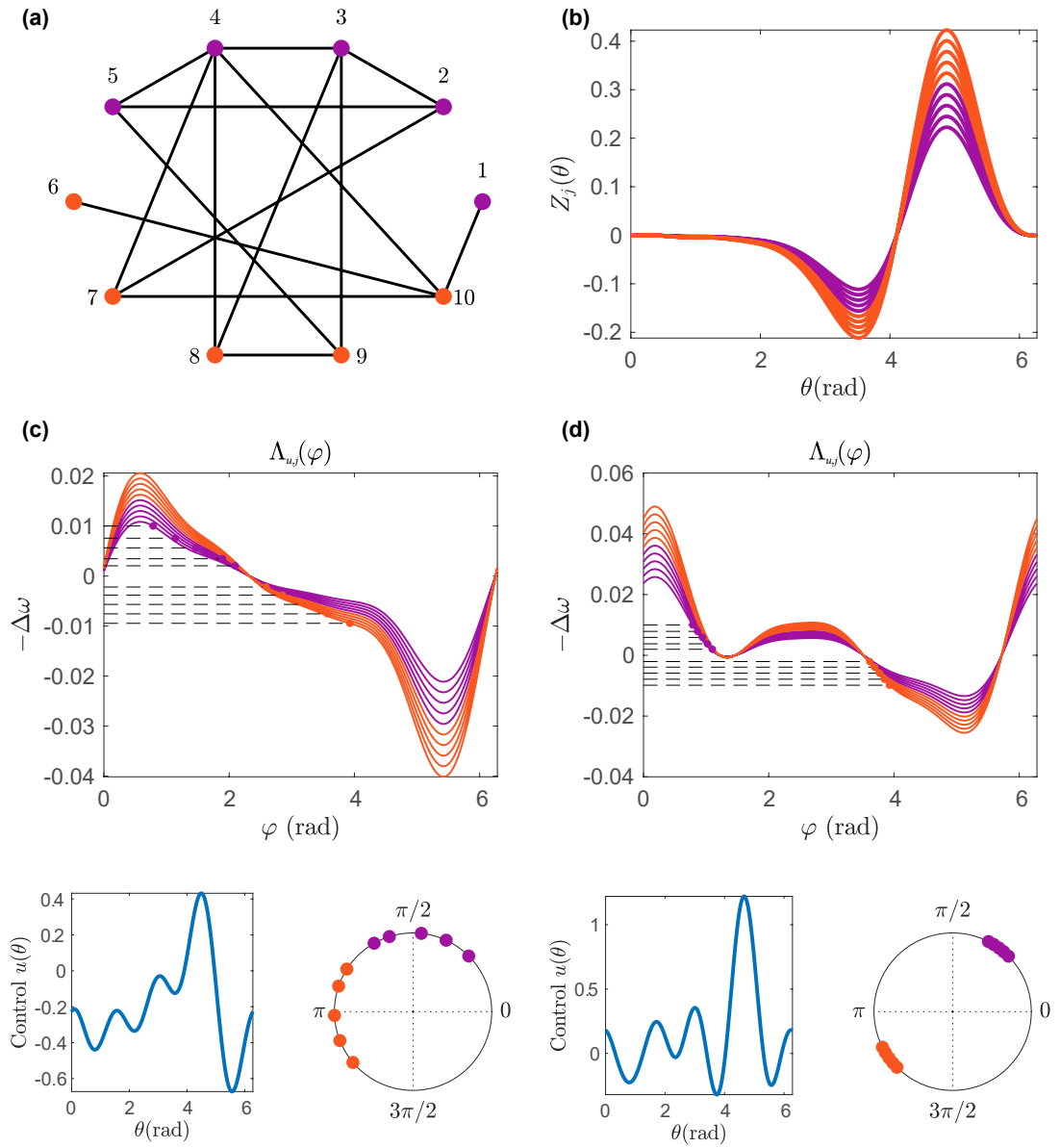

Figure 5.1. *Phase-selective entrainment of a coupled oscillatory network. (a) Network topology (b) PRCs of the oscillators in the network. The top panels of (c) and (d) display the designed optimal interaction function to achieve uniform phase distribution in* $[\pi/4, 5\pi/4]$ *and to construct two clusters at* $\pi/4$ *and* $5\pi/4$ *with 5 oscillators in each cluster. The bottom panels of (c) and (d) illustrate the respective control input (left) and the achieved phase pattern on a unit circle (right). All the oscillators in the network have identical initial phases at 0. Oscillator's frequencies are uniformly distributed in* $[9.99, 10.01]$ *rad/s with the oscillator* 1 *being the slowest and* 10 *being the fastest; the periodic input is of frequency* 10 *rad/s. Network is coupled with sinusoidal coupling function such that* $\alpha_{ij} = 0.0002\sin(\psi_j - \psi_i)$.

$[9.99, 10.01] rad/s$ and PRCs are shown in Figure 5.1(b), where PRCs with smaller amplitudes belong to the slower oscillators. We entrain the oscillators in two particular phase configura-

tions: uniform entrainment phases in $[\pi/4, 5\pi/4]$ and two clusters at $\pi/4$ and $5\pi/4$ with each cluster having 5 oscillators. The optimal interaction functions corresponding to the uniform phase distribution and cluster formation are displayed in the top panels of the Figure 5.1(c) and (d), respectively, while the bottom panels depict the respective control input (left) and resulting entrainment phases (right).

6. Conclusions. In this paper, we present a framework for optimal entrainment of an ensemble of heterogeneous oscillators to form desired stable phase patterns by leveraging the phase model description of oscillators. We show that complex tasks of phase-selective entrainment can be reduced to a compact, tractable quadratic optimization problem. This approach not only enables us to entrain oscillators with heterogeneous PRCs but also provides a new paradigm to design optimal entrainment controls for versatile objectives, which expands the scope of the state-of-the-art techniques that are limited to control oscillators with identical PRCs. In addition, the presented control technique is theoretically robust and practically applicable as we only require the natural frequencies and PRCs of the ensemble, both of which can be measured experimentally with high precision. The optimization framework permits the incorporation of additional experimental restrictions on the control input, such as maximum amplitude. Such a degree of freedom is essential when controlling biological ensembles, where physiological and experimental constraints restrict the range of possible inputs. Furthermore, the optimality of control inputs, e.g., minimum-power stimuli, is critical from both a theoretical and physiological viewpoint. From the physiological aspect, such optimal controls are ideal for treating neurological disorders, where strong inputs may damage brain cells; and from the theoretical perspective, they are required when employing phase models as weak forcing is an underlying assumption for phase model validity. We believe the framework presented here provides an alternative and effective set of numerical tools for examining how variation in oscillator properties, such as natural frequency and PRC, affects the range of entrainment.

Appendix A. Entrainment of a single oscillator.

To entrain an oscillator with a periodic input of frequency Ω at phase φ^* with minimum entrainment speed $|h|$, first, we design the optimal interaction function using (4.9). Afterward, we evaluate the Fourier coefficients of control input using (4.5). On a closer inspection, we note if the PRC contains more than 1 non-zero Fourier coefficients, an optimal control signal to entrain the oscillator at a phase φ^* always exists and is given by

$$u(\theta) = -\frac{\Delta\omega}{\langle Z^2\rangle} Z(\theta+\varphi^*) + \frac{h}{\langle Z'^2\rangle} Z'(\theta+\varphi^*), \tag{A.1}$$

where $\langle\,\cdot\,\rangle$ is an average operator on 2π-periodic functions, and Z' is the first-order derivative of PRC Z. It can be shown using Fourier series representation that $\langle ZZ'\rangle = 0$, which gives us input power $\langle u^2\rangle = \frac{\Delta\omega^2}{\langle Z^2\rangle} + \frac{h^2}{\langle Z'^2\rangle}$. The optimal input power is proportional to the square of the local entrainment speed for a given frequency detuning. Furthermore, for marginal entrainment, i.e., $h = 0$, the square root of input power $\sqrt{\langle u^2\rangle}$ is proportional to the frequency detuning demonstrating the relationship between the range of entrainment and minimum input power, also known as Arnold Tongue [25]. For given input power, the range of input periods over which entrainment occurs is called the "range of entertainment" [33].

Proof. Suppose the inequality constraint in the optimization problem (4.9) is inactive, i.e., $G\boldsymbol{y} = \bar{h} < h$. Then, the optimal entrainment function can be obtained by

$$\begin{aligned} \min \quad & \frac{1}{2}\boldsymbol{y}^T Q \boldsymbol{y} \\ \text{s.t.} \quad & \begin{bmatrix} G \\ A \end{bmatrix} \boldsymbol{y} = \begin{bmatrix} \bar{h} \\ -\Delta\omega \end{bmatrix}. \end{aligned} \tag{A.2}$$

The minimizer of (A.2) is given by [3]

$$\boldsymbol{y} = Q^{-1} \begin{bmatrix} G^T & A^T \end{bmatrix} \left(\begin{bmatrix} G \\ A \end{bmatrix} Q^{-1} \begin{bmatrix} G^T & A^T \end{bmatrix} \right)^{-1} \begin{bmatrix} \bar{h} \\ -\Delta\omega \end{bmatrix}. \tag{A.3}$$

The matrices $G, A \in \mathbb{R}^{1\times(2r+1)}$ are constructed such that $G\boldsymbol{y} = \Lambda_u'(\varphi^*)$ and $A\boldsymbol{y} = \Lambda_u(\varphi^*)$, the matrix Q is given by (4.6), and r is the number of PRC Fourier harmonics. After substituting the values of matrices G, A, and Q,

$$\boldsymbol{y} = Q^{-1} \begin{bmatrix} 0 & 1 \\ -\sin(\varphi^*) & \cos(\varphi^*) \\ \cos(\varphi^*) & \sin(\varphi^*) \\ \vdots & \vdots \\ -r\sin(r\varphi^*) & \cos(r\varphi^*) \\ r\cos(r\varphi^*) & \sin(r\varphi^*) \end{bmatrix} \begin{bmatrix} \frac{\langle Z'^2\rangle}{2} & 0 \\ 0 & \frac{\langle Z^2\rangle}{2} \end{bmatrix}^{-1} \begin{bmatrix} \bar{h} \\ -\Delta\omega \end{bmatrix}.$$

After some further simplifications, the elements of vector $\boldsymbol{y}$ can be obtained as

$$\begin{aligned} f_0 &= -\frac{\Delta\omega}{\langle Z^2\rangle} a_0^2, \\ f_n &= \frac{a_n^2 + b_n^2}{2} \left(-\frac{\Delta\omega}{\langle Z^2\rangle} \cos n\varphi^* - \frac{\bar{h}}{\langle Z'^2\rangle} n \sin n\varphi^* \right), \\ g_n &= \frac{a_n^2 + b_n^2}{2} \left(-\frac{\Delta\omega}{\langle Z^2\rangle} \sin n\varphi^* + \frac{\bar{h}}{\langle Z'^2\rangle} n \cos n\varphi^* \right). \end{aligned}$$

Consequently, using (4.5), the input Fourier coefficients can be expressed as

$$\begin{aligned} c_0 &= -\frac{\Delta\omega}{\langle Z^2\rangle} a_0, \\ c_n &= -\frac{\Delta\omega}{\langle Z^2\rangle} \left(a_n \cos n\varphi^* + b_n \sin n\varphi^* \right) + \frac{n\bar{h}}{\langle Z'^2\rangle} \left(b_n \cos n\varphi^* - a_n \sin n\varphi^* \right), \\ d_n &= -\frac{\Delta\omega}{\langle Z^2\rangle} \left(b_n \cos n\varphi^* - a_n \sin n\varphi^* \right) - \frac{n\bar{h}}{\langle Z'^2\rangle} \left(a_n \cos n\varphi^* + b_n \sin n\varphi^* \right). \end{aligned}$$

The control input, $u(\theta) = c_0 + \sum_{n=1}^{r} c_n \cos n\theta + d_n \sin n\theta$, can be written as a linear combination of shifted PRC and derivative of PRC after substituting the estimated Fourier coefficients, giving us

$$u(\theta) = -\frac{\Delta\omega}{\langle Z^2\rangle} Z(\theta + \varphi^*) + \frac{\bar{h}}{\langle Z'^2\rangle} Z'(\theta + \varphi^*).$$

Correspondingly, the power of input signal $\langle u^2\rangle = \frac{\Delta\omega^2}{\langle Z^2\rangle} + \frac{\bar{h}^2}{\langle Z'^2\rangle}$. Note that the value of $\bar{h}$ is unknown in the expression of control input. However, $\bar{h} < h \leq 0 \implies \bar{h}^2 > h^2$, so the minimum-power control will be obtained when inequality constraint is active, i.e., $G\boldsymbol{y} = h$, which gives us

$$u(\theta) = -\frac{\Delta\omega}{\langle Z^2\rangle} Z(\theta+\varphi^*) + \frac{h}{\langle Z'^2\rangle} Z'(\theta+\varphi^*).$$

Appendix B. Anti-phase entrainment of two oscillators.

Our objective is to design a optimal power control of frequency Ω such that a system of two oscillators with frequencies ω_1, ω_2 is entrained at phases φ_1^* and φ_2^*, where $\varphi_2^* - \varphi_1^* = \pi$. We assume that the Fourier approximation of PRC contains a sufficient number of harmonics to ensure a nonempty feasible region in (4.9). To begin, suppose the inequality constraints in (4.9) are inactive, i.e. $G\boldsymbol{y} = \begin{bmatrix}\bar{h}_1\\ \bar{h}_2\end{bmatrix}$, where $\bar{h}_1, \bar{h}_2 \leq 0$ (we take $h_1, h_2 = 0$, and PRCs are assumed to be identical). Then, the optimal interaction function coefficients can be obtained by

$$\begin{aligned} &\min \quad \frac{1}{2}\boldsymbol{y}^T Q \boldsymbol{y} \\ &\text{s.t.} \quad \begin{bmatrix}G\\ A\end{bmatrix}\boldsymbol{y} = \begin{bmatrix}\bar{h}_1\\ \bar{h}_2\\ -\Delta\omega_1\\ -\Delta\omega_2\end{bmatrix}. \end{aligned} \tag{B.1}$$

The minimizer of (B.1) is given by [3]

$$\boldsymbol{y} = Q^{-1}\begin{bmatrix}G^T & A^T\end{bmatrix}\left(\begin{bmatrix}G\\ A\end{bmatrix} Q^{-1}\begin{bmatrix}G^T & A^T\end{bmatrix}\right)^{-1}\begin{bmatrix}\bar{h}_1\\ \bar{h}_2\\ -\Delta\omega_1\\ -\Delta\omega_2\end{bmatrix}. \tag{B.2}$$

Using (B.2), the minimum control power

$$\frac{1}{2}\boldsymbol{y}^T Q\boldsymbol{y} = \begin{bmatrix}\bar{h}_1 & \bar{h}_2 & -\Delta\omega_1 & -\Delta\omega_2\end{bmatrix}\left(\begin{bmatrix}G\\ A\end{bmatrix} Q^{-1}\begin{bmatrix}G^T & A^T\end{bmatrix}\right)^{-1}\begin{bmatrix}\bar{h}_1\\ \bar{h}_2\\ -\Delta\omega_1\\ -\Delta\omega_2\end{bmatrix}.$$

After substituting the expressions of matrices G, A, and Q, we get

$$\frac{1}{2}\boldsymbol{y}^T Q\boldsymbol{y} = \begin{bmatrix}\bar{h}_1 & \bar{h}_2 & -\Delta\omega_1 & -\Delta\omega_2\end{bmatrix}\begin{bmatrix}\frac{\langle Z'^2\rangle}{2} & \beta & 0 & 0\\ \beta & \frac{\langle Z'^2\rangle}{2} & 0 & 0\\ 0 & 0 & \frac{\langle Z^2\rangle}{2} & \alpha\\ 0 & 0 & \alpha & \frac{\langle Z^2\rangle}{2}\end{bmatrix}^{-1}\begin{bmatrix}\bar{h}_1\\ \bar{h}_2\\ -\Delta\omega_1\\ -\Delta\omega_2\end{bmatrix},$$

where

$$\alpha = \frac{a_0^2}{2} + \sum_{n=1}^{r} (-1)^n \frac{a_n^2 + b_n^2}{4}, \qquad \beta = \sum_{n=1}^{r} (-1)^n n^2 \frac{a_n^2 + b_n^2}{4}.$$

We can further simplify the expression by using the block matrix inversion formula. After taking the inverse and simplifying the above expression, we get

$$\frac{1}{2}\boldsymbol{y}^T Q \boldsymbol{y} = \frac{1}{\gamma}\begin{bmatrix}\bar{h_1} & \bar{h_2}\end{bmatrix}\begin{bmatrix}\frac{\langle Z'^2\rangle}{2} & -\beta \\ -\beta & \frac{\langle Z'^2\rangle}{2}\end{bmatrix}\begin{bmatrix}\bar{h_1} \\ \bar{h_2}\end{bmatrix} + \frac{1}{\delta}\begin{bmatrix}-\Delta\omega_1 & -\Delta\omega_2\end{bmatrix}\begin{bmatrix}\frac{\langle Z^2\rangle}{2} & -\alpha \\ -\alpha & \frac{\langle Z^2\rangle}{2}\end{bmatrix}\begin{bmatrix}-\Delta\omega_1 \\ -\Delta\omega_2\end{bmatrix},$$

where $\gamma = \frac{\langle Z'^2\rangle^2}{4} - \beta^2$, and $\delta = \frac{\langle Z^2\rangle^2}{4} - \alpha^2$. Note that the matrix $\begin{bmatrix}\frac{\langle Z'^2\rangle}{2} & -\beta \\ -\beta & \frac{\langle Z'^2\rangle}{2}\end{bmatrix}$ is a positive-definite matrix which means that the control power will be minimum when $\bar{h_1} = \bar{h_2} = 0$. We can obtain optimal interaction function coefficients, by substituting $\bar{h_1} = \bar{h_2} = 0$ in (B.2), as

$$\boldsymbol{y} = Q^{-1}\begin{bmatrix}G^T & A^T\end{bmatrix}\begin{bmatrix}\frac{\langle Z'^2\rangle}{2} & \beta & 0 & 0 \\ \beta & \frac{\langle Z'^2\rangle}{2} & 0 & 0 \\ 0 & 0 & \frac{\langle Z^2\rangle}{2} & \alpha \\ 0 & 0 & \alpha & \frac{\langle Z^2\rangle}{2}\end{bmatrix}^{-1}\begin{bmatrix}0 \\ 0 \\ -\Delta\omega_1 \\ -\Delta\omega_2\end{bmatrix} = Q^{-1}A^T\begin{bmatrix}2a \\ 2b\end{bmatrix},$$

where

$$a = \frac{1}{2\left(\frac{\langle Z^2\rangle^2}{4} - \alpha^2\right)}\left(-\frac{\langle Z^2\rangle}{2}\Delta\omega_1 + \alpha\Delta\omega_2\right),$$
$$b = \frac{1}{2\left(\frac{\langle Z^2\rangle^2}{4} - \alpha^2\right)}\left(-\frac{\langle Z^2\rangle}{2}\Delta\omega_2 + \alpha\Delta\omega_1\right).$$

By further solving the above equation, we get

$$f_0 = a_0^2(a+b),$$
$$f_n = \frac{a_n^2 + b_n^2}{2}\left(a\cos n\varphi_1^* + b\cos n\varphi_2^*\right),$$
$$g_n = \frac{a_n^2 + b_n^2}{2}\left(a\sin n\varphi_1^* + b\sin n\varphi_2^*\right),$$

where $[f_0, f_1, g_1, \ldots, f_r, g_r]$ are the elements of vector $\boldsymbol{y}$. Following the derivation in Appendix A, we can write the control input as

$$u(\theta) = aZ(\theta + \varphi_1^*) + bZ(\theta + \varphi_2^*). \tag{B.3}$$

From the control input expression, we can also obtain control power $\langle u^2\rangle = a^2\langle Z^2\rangle + b^2\langle Z^2\rangle + 2ab\alpha$.

Appendix C. Implementability of the optimal input as a pulse train.

Here, we provide a simple procedure for implementing the proposed optimal input as a pulse train, which are standard DBS inputs. We illustrate this approach on the examples presented in Section 4.4. The pulse train frequency and pulse width are taken as 200 Hz and 1ms, which are typical settings for a high frequency DBS [37, 45] and the pulse amplitude is determined by the sampled value of reference signal, i.e., control generated by our algorithm, at the instant when pulse is applied (see Figure C.1).

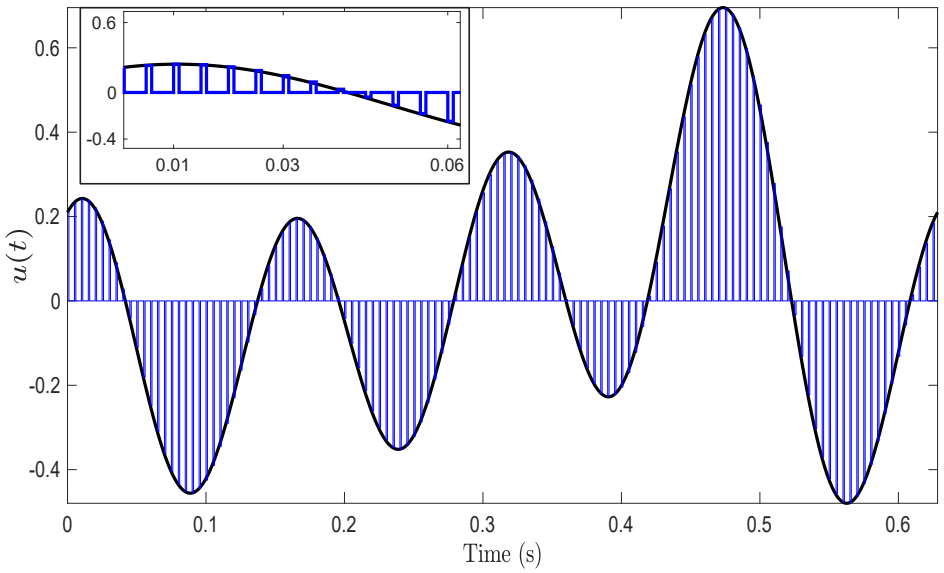

Figure C.1. *Implementation of the optimal input (black) as a pulse train (blue). The inset figure displays a zoomed view.*

Note that the generated pulse train, say $p(t)$, will have less power than the optimal input. To incorporate this loss of power, we further multiply $p(t)$ by a constant c such that the pulse train energy is no less than the optimal input to ensure the entrainment of oscillators to the pulse train. The resulting pulse train, $c \times p(t)$, is then applied to the examples of Section 4.4 and the final entrainment phases are shown in Figure C.2 where the cross mark denotes the desired phases.

REFERENCES

[1] M. Abramowitz, I. A. Stegun, and R. H. Romer, *Handbook of mathematical functions with formulas, graphs, and mathematical tables*, 1988.
[2] D. Avitabile, P. Słowiński, B. Bardy, and K. Tsaneva-Atanasova, *Beyond in-phase and anti-phase coordination in a model of joint action*, Biological cybernetics, 110 (2016), pp. 201–216.
[3] S. Boyd and L. Vandenberghe, *Convex Optimization*, Cambridge University Press, 2004.
[4] S. D. Burton, G. B. Ermentrout, and N. N. Urban, *Intrinsic heterogeneity in oscillatory dynamics limits correlation-induced neural synchronization*, Journal of Neurophysiology, 108 (2012), pp. 2115–2133.
[5] G. Buzsáki, *Rhythms of the Brain*, Oxford University Press, 2006.

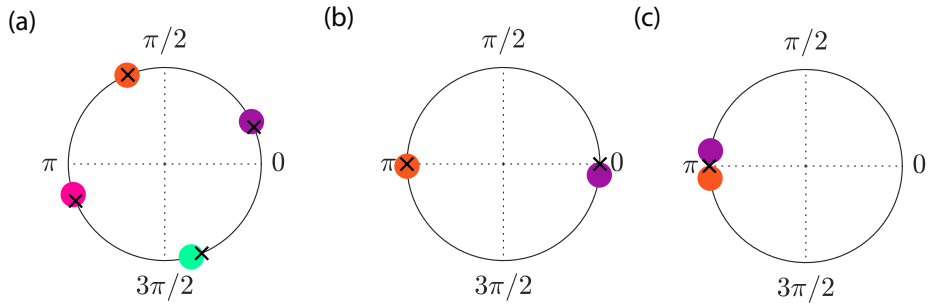

Figure C.2. *Entrainment phases when the optimal control is implemented via a pulse train. (a) Final entrainment phases for numerical example demonstrating the desynchronization of Hodgkin-Huxley phase oscillators. Panels (b) and (c) display entrainment phases corresponding to the anti-phase and in-phase entrainment of Type-1 and Type-2 PRC oscillators.*

[6] R. Cestnik and M. Rosenblum, *Inferring the phase response curve from observation of a continuously perturbed oscillator*, Scientific reports, 8 (2018), p. 13606.

[7] M. F. Crowley and R. J. Field, *Electrically coupled belousov-zhabotinskii oscillators. 1. experiments and simulations*, The Journal of Physical Chemistry, 90 (1986), pp. 1907–1915.

[8] I. S. Dasanayake and J.-S. Li, *Constrained charge-balanced minimum-power controls for spiking neuron oscillators*, Systems & Control Letters, 75 (2015), pp. 124–130.

[9] H. O. de la Iglesia, T. Cambras, W. J. Schwartz, and A. Díez-Noguera, *Forced desynchronization of dual circadian oscillators within the rat suprachiasmatic nucleus*, Current biology, 14 (2004), pp. 796–800.

[10] B. Ermentrout, *Type i membranes, phase resetting curves, and synchrony*, Neural computation, 8 (1996), pp. 979–1001.

[11] R. F. Galán, G. B. Ermentrout, and N. N. Urban, *Efficient estimation of phase-resetting curves in real neurons and its significance for neural-network modeling*, Physical review letters, 94 (2005), p. 158101.

[12] C. Gu, M. Tang, and H. Yang, *The synchronization of neuronal oscillators determined by the directed network structure of the suprachiasmatic nucleus under different photoperiods*, Scientific Reports, 6 (2016), p. 28878.

[13] S. Hanslmayr and T. Staudigl, *How brain oscillations form memories—a processing based perspective on oscillatory subsequent memory effects*, Neuroimage, 85 (2014), pp. 648–655.

[14] F. C. Hoppensteadt and E. M. Izhikevich, *Weakly Connected Neural Networks*, Springer New York, 1997.

[15] Y. Kato, A. Zlotnik, J.-S. Li, and H. Nakao, *Optimization of periodic input waveforms for global entrainment of weakly forced limit-cycle oscillators*, Nonlinear Dynamics, 105 (2021), pp. 2247–2263.

[16] I. Z. Kiss, C. G. Rusin, H. Kori, and J. L. Hudson, *Engineering complex dynamical structures: Sequential patterns and desynchronization*, Science, 316 (2007), pp. 1886–1889.

[17] I. Z. Kiss, Y. Zhai, and J. L. Hudson, *Predicting mutual entrainment of oscillators with experiment-based phase models*, Physical review letters, 94 (2005), p. 248301.

[18] I. Z. Kiss, Y. Zhai, and J. L. Hudson, *Resonance clustering in globally coupled electrochemical oscillators with external forcing*, Physical Review E, 77 (2008), p. 046204.

[19] E. P. Leitgeb, M. Šterk, T. Petrijan, P. Gradišnik, and M. Gosak, *The brain as a complex network: assessment of eeg-based functional connectivity patterns in patients with childhood absence epilepsy*, Epileptic Disorders, 22 (2020), pp. 519–530.

[20] C. R. McClung, *The genetics of plant clocks*, Advances in genetics, 74 (2011), pp. 105–139.

[21] D. Morse, J. W. Hastings, and T. Roenneberg, *Different phase responses of the two circadian oscillators in gonyaulax*, Journal of biological rhythms, 9 (1994), pp. 263–274.

[22] A. V. Oppenheim, A. S. Willsky, and S. H. Nawab, *Signals & Systems*, Prentice-Hall, Inc., USA, 1996.
[23] M. G. Pedersen, E. Mosekilde, K. S. Polonsky, and D. S. Luciani, *Complex patterns of metabolic and ca2+ entrainment in pancreatic islets by oscillatory glucose*, Biophysical journal, 105 (2013), pp. 29–39.
[24] B. Pietras and A. Daffertshofer, *Network dynamics of coupled oscillators and phase reduction techniques*, Physics Reports, 819 (2019), pp. 1–105.
[25] A. Pikovsky, M. Rosenblum, and J. Kurths, *Synchronization - A Universal Concept in Nonlinear Sciences*, vol. 12 of Cambridge Nonlinear Science Series, Cambridge University Press, 2001.
[26] T. Roenneberg, S. Daan, and M. Merrow, *The art of entrainment*, Journal of biological rhythms, 18 (2003), pp. 183–194.
[27] M. Rosenblum et al., *Reconstructing networks of pulse-coupled oscillators from spike trains*, Physical Review E, 96 (2017), p. 012209.
[28] A. Sirota, S. Montgomery, S. Fujisawa, Y. Isomura, M. Zugaro, and G. Buzsáki, *Entrainment of neocortical neurons and gamma oscillations by the hippocampal theta rhythm*, Neuron, 60 (2008), pp. 683–697.
[29] R. M. Smeal, G. B. Ermentrout, and J. A. White, *Phase-response curves and synchronized neural networks*, Philosophical Transactions of the Royal Society B: Biological Sciences, 365 (2010), pp. 2407–2422.
[30] K. M. Spencer, P. G. Nestor, M. A. Niznikiewicz, D. F. Salisbury, M. E. Shenton, and R. W. McCarley, *Abnormal neural synchrony in schizophrenia*, The Journal of Neuroscience, 23 (2003), pp. 7407–7411.
[31] K. M. Stiefel, B. S. Gutkin, and T. J. Sejnowski, *Cholinergic neuromodulation changes phase response curve shape and type in cortical pyramidal neurons*, PLoS ONE, 3 (2008), p. e3947.
[32] I. T. Tokuda, S. Jain, I. Z. Kiss, and J. L. Hudson, *Inferring phase equations from multivariate time series*, Physical review letters, 99 (2007), p. 064101.
[33] I. T. Tokuda, C. Schmal, B. Ananthasubramaniam, and H. Herzel, *Conceptual models of entrainment, jet lag, and seasonality*, Frontiers in Physiology, 11 (2020), p. 334.
[34] Y. Tsubo, M. Takada, A. D. Reyes, and T. Fukai, *Layer and frequency dependencies of phase response properties of pyramidal neurons in rat motor cortex*, European Journal of Neuroscience, 25 (2007), pp. 3429–3441.
[35] J. P. Velazquez, R. Galán, L. G. Dominguez, Y. Leshchenko, S. Lo, J. Belkas, and R. G. Erra, *Phase response curves in the characterization of epileptiform activity*, Physical Review E, 76 (2007), p. 061912.
[36] A. F. Villaverde, N. Tsiantis, and J. R. Banga, *Full observability and estimation of unknown inputs, states and parameters of nonlinear biological models*, Journal of the Royal Society Interface, 16 (2019), p. 20190043.
[37] J. Volkmann, J. Herzog, F. Kopper, and G. Deuschl, *Introduction to the programming of deep brain stimulators*, Movement disorders: official journal of the Movement Disorder Society, 17 (2002), pp. S181–S187.
[38] K. Wendling and C. Ly, *Firing rate distributions in a feedforward network of neural oscillators with intrinsic and network heterogeneity*, Mathematical Biosciences and Engineering, 16 (2019), pp. 2023–2048.
[39] C. J. Wilson, B. Beverlin, and T. Netoff, *Chaotic desynchronization as the therapeutic mechanism of deep brain stimulation*, Frontiers in Systems Neuroscience, 5 (2011).
[40] D. Wilson, A. B. Holt, T. I. Netoff, and J. Moehlis, *Optimal entrainment of heterogeneous noisy neurons*, Frontiers in neuroscience, 9 (2015), p. 192.
[41] D. Wilson and J. Moehlis, *An energy-optimal approach for entrainment of uncertain circadian oscillators*, Biophysical journal, 107 (2014), pp. 1744–1755.
[42] D. Wilson and J. Moehlis, *Optimal chaotic desynchronization for neural populations*, SIAM Journal on Applied Dynamical Systems, 13 (2014), p. 276.
[43] A. T. Winfree, *Circadian Rhythms in General*, Springer New York, New York, NY, 2001, pp. 545–591.
[44] Y. Xu, Q. S. Padiath, R. E. Shapiro, C. R. Jones, S. C. Wu, N. Saigoh, K. Saigoh, L. J. Ptáček, and Y.-H. Fu, *Functional consequences of a ckiδ mutation causing familial advanced sleep*

phase syndrome, Nature, 434 (2005), pp. 640–644.

[45] Y. Yuan, L. Zheng, Z. Feng, and G. Yang, *Different effects of monophasic pulses and biphasic pulses applied by a bipolar stimulation electrode in the rat hippocampal ca1 region*, BioMedical Engineering OnLine, 20 (2021), pp. 1–12.

[46] C. Zhang and T. J. Lewis, *Phase response properties of half-center oscillators*, Journal of computational neuroscience, 35 (2013), pp. 55–74.

[47] A. Zlotnik, Y. Chen, I. Z. Kiss, H.-A. Tanaka, and J.-S. Li, *Optimal waveform for fast entrainment of weakly forced nonlinear oscillators*, Physical review letters, 111 (2013), p. 024102.

[48] A. Zlotnik and J.-S. Li, *Optimal entrainment of neural oscillator ensembles*, Journal of neural engineering, 9 (2012), p. 046015.

[49] A. Zlotnik, R. Nagao, I. Z. Kiss, and J.-S. Li, *Phase-selective entrainment of nonlinear oscillator ensembles*, Nature communications, 7 (2016), pp. 1–7.